Received: 18 June 2023 | Revised: 14 October 2023 | Accepted: 17 November 2023

DOI: 10.1002/pro.4843

RESEARCH ARTICLE

THE PROTEIN SOCIETY WILEY

Molecular interactions between perlecan LG3 and the SARS-CoV-2 spike protein receptor binding domain

Timothy E. Gressett[1,2] | **Md Lokman Hossen**[3,4] | **Grant Talkington**[1,2] | **Milla Volic**[1] | **Hugo Perez**[3] | **Purushottam B. Tiwari**[5] | **Prem Chapagain**[3,6] | **Gregory Bix**[1,2,7,8]

[1]Department of Neurosurgery, Clinical Neuroscience Research Center, Tulane University School of Medicine, New Orleans, Louisiana, USA

[2]Tulane Brain Institute, Tulane University, New Orleans, Louisiana, USA

[3]Department of Physics, Florida International University, Miami, Florida, USA

[4]Department of Physics, University of Barishal, Kornokathi, Bangladesh

[5]Department of Oncology, Georgetown University School of Medicine, Washington, DC, USA

[6]Biomolecular Sciences Institute, Florida International University, Miami, Florida, USA

[7]Department of Neurology, Tulane University School of Medicine, New Orleans, Louisiana, USA

[8]Department of Microbiology and Immunology, Tulane University School of Medicine, New Orleans, Louisiana, USA

Correspondence
Prem Chapagain, Department of Physics, Florida International University, Miami, FL 33199, USA.
Email: chapagap@fiu.edu

Gregory Bix, Department of Neurosurgery, Clinical Neuroscience Research Center, Tulane University School of Medicine, New Orleans, LA 70112, USA.
Email: gbix@tulane.edu

Funding information
National Institute of Health, Grant/Award Number: P30CA51008; Tulane University

Review Editor: Nir Ben-Tal

Abstract

Severe acute respiratory syndrome coronavirus-2 (SARS-CoV-2) has caused a global health crisis with significant clinical morbidity and mortality. While angiotensin-converting enzyme 2 (ACE2) is the primary receptor for viral entry, other cell surface and extracellular matrix proteins may also bind to the viral receptor binding domain (RBD) within the SARS-CoV-2 spike protein. Recent studies have implicated heparan sulfate proteoglycans, specifically perlecan LG3, in facilitating SARS-CoV-2 binding to ACE2. However, the role of perlecan LG3 in SARS-CoV-2 pathophysiology is not well understood. In this study, we investigated the binding interactions between the SARS-CoV-2 spike protein RBD and perlecan LG3 through molecular modeling simulations and surface plasmon resonance (SPR) experiments. Our results indicate stable binding between LG3 and SARS-CoV-2 spike protein RBD, which may potentially enhance RBD-ACE2 interactions. These findings shed light on the role of perlecan LG3 in SARS-CoV-2 infection and provide insight into SARS-CoV-2 pathophysiology and potential therapeutic strategy for COVID-19.

KEYWORDS

extracellular matrix, heparan sulfate proteoglycan, LG3, molecular dynamics, perlecan, SARS-CoV-2, surface plasmon resonance

Timothy E. Gressett and Md Lokman Hossen contributed equally as first authors.

1 | INTRODUCTION

Severe acute respiratory syndrome coronavirus-2 (SARS-CoV-2) has caused a global health crisis with significant clinical morbidity and mortality since its emergence (Zhang et al., 2023). Although angiotensin-converting enzyme 2 (ACE2) is recognized as the primary functional receptor for SARS-CoV-2 viral entry, a variety of cell surface and extracellular matrix (ECM) proteins have demonstrated binding affinity for the SARS-CoV-2 receptor binding domain (RBD) (Brodowski et al., 2022; Iacobucci et al., 2022; Kadam et al., 2021; Norris et al., 2023). The degree to which these molecules may modulate infectivity, however, remains unknown.

Recent studies have suggested that negatively charged heparan sulfate (HS) proteoglycans may be cofactors for SARS-CoV-2 binding to ACE2, where HS moieties interact with the RBD on the "spike" or S protein to open its conformation to allow for enhanced binding to ACE2 (Clausen et al., 2020; Lo et al., 2022). This negatively charged HS moiety is expressed ubiquitously within the ECM proteoglycan perlecan, which is abundantly located in the vascular basement membrane of endothelial cells as well as in a diverse array of other tissues. Perlecan plays a role in various biological functions such as lipid metabolism, angiogenesis, cell adhesion, endocytosis, and autophagy (Gubbiotti et al., 2017). Perlecan is one of the largest proteoglycans ever discovered, with a 500 kDa protein core encoded by a 120 KB gene (*HSPG2*) divided into 97 exons. The core protein possesses 5 domains, each with its own function and binding nature: domain I, exhibiting the greatest level of HS post-translation modification of any domain, participates in ligand-receptor interactions facilitating angiogenesis, domain II in lipid retention, domain III in cell surface binding, domain IV in scaffold integrity, and domain V in cell surface binding and induction of autophagy (Martinez et al., 2018; Melrose, 2020). Domain V of perlecan consists of three laminin globular domain-like regions (LG1, LG2, and LG3), which are arranged in tandem repeats interspersed by two EGF-like domains (EG) (Melrose, 2020). Domain V can be liberated from perlecan via matrix metalloproteinases and further cleaved into LG3 by Cathepsin L and BMP-1-Toilloid-Like proteases (Gonzalez et al., 2005). Once cleaved, LG3 binds to integrin receptors to produce an anti-angiogenic effect through the disruption of focal adhesions and the actin cytoskeleton (Hayes et al., 2022). Although it is known that HS may play a role in SARS-CoV-2 host cell attachment, fusion, and intracellular pathways (Yu et al., 2020), the role that perlecan LG3 may have in SARS-CoV-2 pathophysiology remains unclear.

In this work, we investigated the binding interactions between the SARS-CoV-2 spike protein receptor-binding domain (RBD) and human recombinant perlecan LG3 through molecular modeling simulations. We then used molecular docking to select the best candidate complexes and combined our results with molecular dynamics (MD) simulations to investigate LG3 interactions with the spike protein RBD with and without the presence of ACE2. Finally, we followed up these computational investigations with surface plasmon resonance (SPR) experiments to further elucidate potential interactions between SARS-CoV-2 spike protein RBD, ACE2 receptor, and perlecan LG3. Our results indicate a potential role for perlecan LG3 in SARS-CoV-2 pathophysiology and suggest a novel unexplored mechanism which may yield future insight into therapeutic strategy.

2 | MATERIALS AND METHODS

2.1 | Proteins

Wild-type SARS-CoV-2 RBD (SARS-CoV-2 RBD-Wt) and Human ACE2 (hACE2) were purchased from Acro Biosystems (CAT# SPD-C52H3, CAT# AC2-H5257, purity >95% as determined by SDS-PAGE). Perlecan LG3 was manufactured as previously published (Biose et al., 2022). Briefly, human recombinant LG3 was expressed in *E. coli* [BL21(DE3)] utilizing an expression plasmid driven by the T7 polymerase promoter, and purification was achieved by standard clarification of lysis, followed by two column chromatography steps demonstrating approximately 90%–95% purity as measured by reverse phase liquid chromatography mass spectrometry. Endotoxin was determined to be ≤10 EU/mg. Absense of post-translational heparan sulfate linkage was confirmed via proteomic analysis between full-length DV and LG3 fragments manufactured as previously described (Biose et al., 2023).

2.2 | Molecular docking and molecular dynamics simulations

The protein structures of the Ca^{2+} bound LG3, as well as the SARS-CoV-2 RBD, were retrieved from the RCSB Protein Data Bank (Berman et al., 2000) (PDB IDs 3SH5 (Le et al., 2011) and 6VSB (Wrapp et al., 2020) respectively). Molecular template-based protein–protein docking was performed to obtain the LG3-RBD complexes using the web-based docking interface HDOCK (Yan et al., 2020). The complexes were solvated in a cubic box with TIP3 water (Jorgensen et al., 1983) and were

neutralized with 150 mM of KCl using the CHARMM-GUI solution builder interface (Jo et al., 2008; Lee et al., 2016) (Table S1). All-atom, unbiased MD simulations were performed with CHARMM36m force field (Best et al., 2012; Vanommeslaeghe et al., 2010) using the GPU-based simulation package NAMD2.14 (Phillips et al., 2005). The particle mesh Ewald method (Darden et al., 1993; Essmann et al., 1995) was used to calculate the long-range ionic interactions with a nonbonded cutoff 12 Å. Pressure and temperature were controlled with a piston period of 50 fs and decay of 25 fs, and Langevin temperature coupling with a friction coefficient of 1 ps^{-1}, respectively, using the Nose–Hoover Langevin-piston method (Feller et al., 1995; Martyna et al., 1994). We used the SHAKE algorithm (Ryckaert et al., 1977) to fix the hydrogen atoms' covalent bonds. A 10,000-step energy minimization was performed, followed by equilibration and production runs at 303.15 K temperature with a 2 fs time step. The LG3-RBD complexes were simulated for 600 ns each. The simulation for Model 2 was extended to 1 μs for two replica runs (i.e., additional 400 ns runs, Replica 1 and Replica 2). The LG3-RBD-ACE2 complex was simulated for 200 ns. The trajectories were visualized and analyzed with visual molecular dynamics (VMD) (Humphrey et al., 1996).

The binding interfaces were evaluated with PIsToN (protein binding interfaces with transformer networks), a recently developed novel deep learning-based approach (Stebliankin et al., 2023) for distinguishing native-like complexes from decoys. In this approach, each protein interface is transformed into a collection of 2D images (interface maps), where each image corresponds to a geometric or biochemical property in which pixel intensity represents the feature values (Figure S1). The model was trained in contrastive learning settings on thousands of native and computationally predicted protein complexes that contain challenging examples. The network achieved state-of-the-art performance in scoring molecular docking complexes.

2.3 | Surface plasmon resonance

All experiments were done using a Biacore T200 instrument with a CM5 chip at 25°C. LG3 was immobilized onto the chip surface as a ligand. hACE2 was also used as a positive control ligand to immobilize onto the same chip surface. SARS-CoV-2 RBD-Wt was used as an analyte to flow over the ligand-immobilized surfaces. All ligands were immobilized using the standard amine coupling chemistry. LG3 was diluted in 10 mM sodium acetate at pH 5.5 and immobilized to a level of ~1750 RU. hACE2 was diluted in 10 mM sodium acetate buffer at pH 4.5 and immobilized to a level of ~12,400 RU. One flow cell (FC1) was used as the reference for these two different ligands immobilized (active) FCs. FC1 was activated and deactivated using the same surface chemistry but no proteins were immobilized. PBS-P (20 mM phosphate buffer pH 7.4, 137 mM NaCl, 2.7 mM KCl, 0.05% v/v surfactant P20) was used as the running buffer during immobilization of the ligands. SARS-CoV-2 RBD-Wt was then injected in various concentrations in the presence of PBS-P. The flow rate of all analyte solutions was maintained at 50 μL/min. A solution containing H_3PO_4 (1:10,000 v/v ratio, H_3PO_4:ddH_2O) was injected for 20 s for surface regeneration. Each analyte concentration was injected in triplicate. SPR sensorgrams obtained for analysis were both blank (PBS-P only signals) and reference (sensorgrams corresponding to the reference FC) subtracted. The SPR sensorgrams were analyzed using a 1:1 kinetics fitting model available in the Biacore T200 evaluation software version 1.0.

3 | RESULTS

LG3 is one of the three LG fragments in human perlecan domain V, which shows high biological activity (Lee et al., 2011). HS chains of perlecan have been shown to interact with SARS-CoV-2 spike protein and enhance the host cell entry (De Pasquale et al., 2021; Lo et al., 2022; Yu et al., 2020). As human LG3 contains no N-glycosylation sites, we explored possible direct interactions of LG3 protein with the SARS-CoV-2 RBD. To investigate the LG3-RBD binding, we first obtained the LG3-RBD complexes and optimized the structures with MD simulations.

3.1 | Molecular models of LG3-RBD and LG3-RBD-ACE2 complexes

To obtain the molecular models of the LG3 complexes, we performed molecular docking using a template-based docking web interface HDOCK (Yan et al., 2020). We selected the top two best-predicted models based on the HDOCK binding scores, Model 1 and Model 2, for further analysis. In addition to having the lowest energy scores, both models had the LG3 bound to the interfaces that were available for binding in the "RBD up" conformation of the Spike protein and did not clash with glycans. We performed MD simulations of these models to optimize the complex structures. Simulations showed that Model 1 is unstable as the RBD dissociates from the complex within 200 ns as shown in Figure 1a, whereas Model 2 is

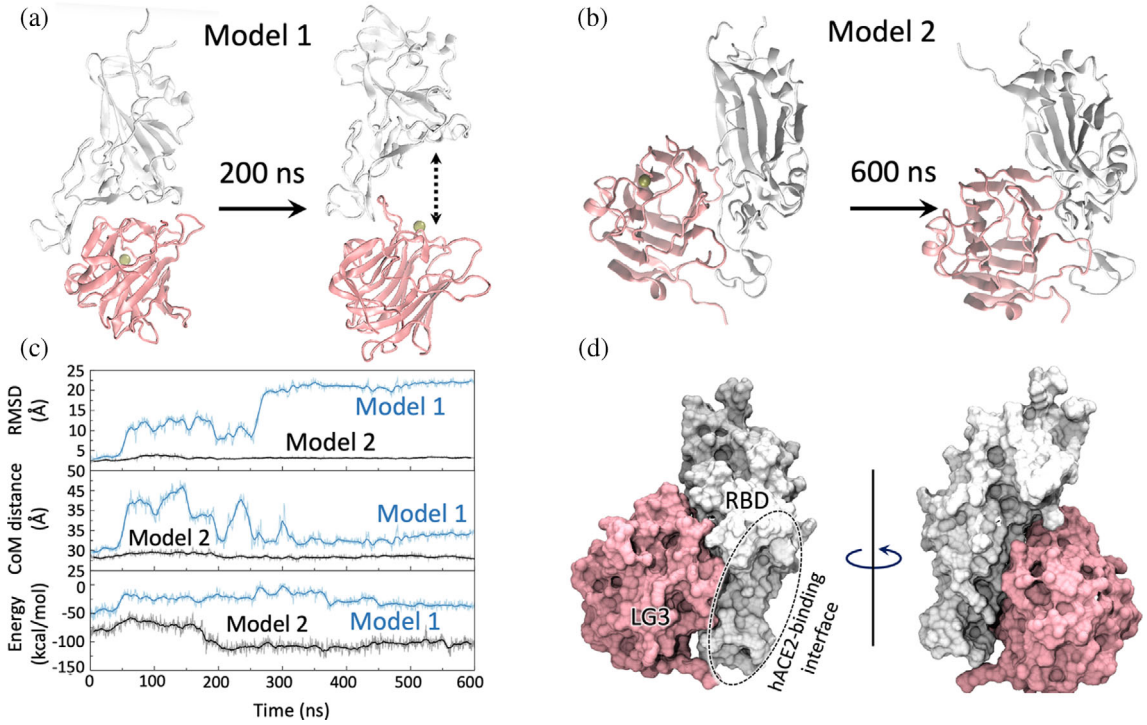

FIGURE 1 Molecular models of LG3-RBD complexes. Docking predicted LG3-RBD complexes of (a) Model 1 complex in which LG3 (pink) binds at the receptor binding interface of the RBD (white) but dissociates within 200 ns of simulation. (b) Model 2 shows a different RBD interface for binding LG3, which yields a stable LG3-RBD complex throughout the 600 ns simulation. (c) Evolution of the root-mean-squared displacement (RMSD) of the complexes and the center-of-mass (CoM) distance between RBD and LG3 in Model 1 and Model 2 during the 600-ns simulations. Also shown is the interaction energy (vdW and coulomb interaction) between LG3 and RBD, calculated using the VMD plugin NAMD energy. (d) LG3-RBD complex from Model 2 is shown from two different orientations rotated by 180°. LG3 binding does not mask the interface for ACE2 binding.

stable throughout the simulation of >600 ns (Figure 1b and Movie S1. The root-mean-squared deviation as well as the distance between the center-of-masses of the RBD and LG3, showing the stable complex for Model 2, is shown in Figure 1c.

Interestingly, LG3 binding at the ACE2-binding interface results in an unstable LG3-RBD complex. In contrast, LG3 binding at a different interface in Model 2 results in a stable LG3-RBD complex. This is also shown by the PIsToN scores (Table S2), calculated based on a deep-learning approach. Model 2 shows the lowest PIsToN score (favorable). In this complex, the ACE2-binding interface of the RBD is not masked (Figure 1d), potentially allowing the RBD to attach to the cell-surface receptor even when LG3 is bound. To explore this possibility and its consequences, we modeled the LG3-RBD-ACE2 complex and performed additional simulations. For this, we took the LG3-RBD complex (Model 2) and aligned the RBD with the RBD of the RBD-ACE2 complex (PDB ID 6VW1 (Shang et al., 2020)). The transformed coordinates of ACE2 were then copied to the LG3-RBD complex to ultimately get the LG3-RBD-ACE2 complex shown in Figure 2. Next, we analyzed the interfacial interactions between LG3 and RBD as well as LG3, RBD, and ACE2.

3.2 | LG3-RBD binding

We analyzed the 600 ns simulation trajectory of the LG3-RBD complex and calculated the inter-protein hydrogen bonds (H-bonds) formed at the interface between LG3 and RBD. The two protein domains make several hydrogen bonds as shown in Figure 3. The strongest contribution to the stability of the complex was found via a salt bridge between E117 (LG3) and R466 (RBD). Other major H-bonds include E35-T470 and E105-S349. The hydrogen-bond forming pairs and their percentage of occupancies are summarized in Figure 3c.

To further confirm the stability of the LG3-RBD, we extended the simulation of the complex to 1.0 μs. We also repeated the simulation from 600 to 1.0 μs. In Figure 4, we plotted the RMSD for the LG3-RBD complex for the extended runs for the two replicas. RMSD (up to 600 ns) is the same as in Figure 1c, but shown on a different scale so that the fluctuations are clearly visible. As the docking

predicted complex relaxes with MD, the RMSD is found to increase up to 100 ns but settles after around 200 ns to a relatively stable state (~3 Å) for the rest of the simulation. The RMSDs for both replicas show a similar pattern.

3.3 | LG3-RBD-ACE2 complex

Since our results suggested LG3-binding at a different interface than the ACE2-binding interface, we investigated the role of LG3 binding on the RBD-ACE2 interactions. We performed MD simulations of the LG3-RBD-ACE2 complex as described earlier (Figure 2), and calculated the H-bonds at the interface between RBD and ACE2 with and without LG3. Figure 5a shows the % occupancy of the RBD-ACE2 H-bonds when LG3 is not bound to the RBD, and Figure 5b shows the % occupancy of the RBD-ACE2 H-bonds when LG3 is bound to the RBD. The H-bonds occupancies appear to be enhanced in the LG3-RBD-ACE2 complex compared to the RBD-ACE2 complex. Specifically, several new hydrogen-bond pairs are observed in the presence of LG3, including A475-Q24, S477-Q24, Y453-H34, and Y505-E37.

We further explored the role of LG3 on the RBD-ACE2 interactions by performing dynamical network analysis (DNA) (Melo et al., 2020) which involves calculating connections (edges) between the amino acids nodes (C_α). The edges among the nodes are calculated based on their correlation matrix when nodes are found to be less than a cutoff value of 4.5 Å for a minimum of 75% of an MD trajectory. Figure 5c, d show the network analysis for the RBD-ACE2 and the LG3-RBD-ACE2 systems. The number of connections between the edges of communities indicates the interaction strength. Figure 5e shows a total of 17 connections at the RBD/ACE2 interface when not complexed with LG3, whereas it shows a total of 24 connections at the RBD/ACE2 interface when the RBD is complexed with LG3 (i.e., for the LG3-RBD-ACE2 complex) in Figure 5f. Thus, DNA calculations of this system support our findings from the H-bond analysis that the presence of LG3 enhances the RBD-ACE2 interactions. While the hydrogen bond and DNA show increased interactions, the actual binding affinity may

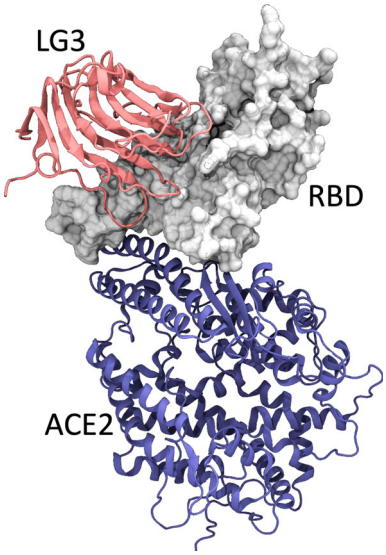

FIGURE 2 LG3-RBD-ACE2 complex obtained by structural alignment of the RBD in the LG3-RBD and RBD-ACE2 complexes. Structural alignment was performed using VMD's MultiSeq tool (Roberts et al., 2006). The resulting complex shows different RBD binding interfaces for LG3 and ACE2.

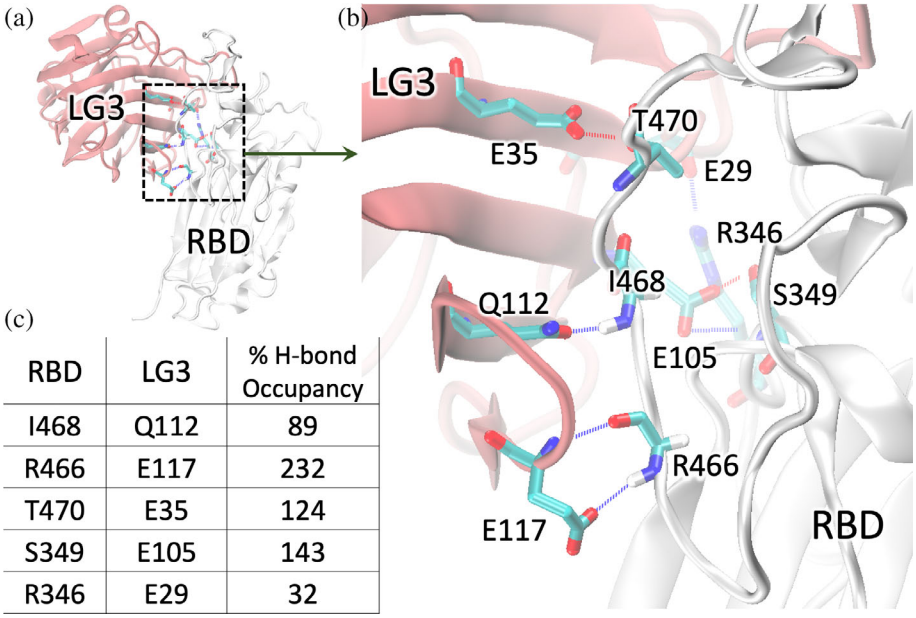

(c)

RBD	LG3	% H-bond Occupancy
I468	Q112	89
R466	E117	232
T470	E35	124
S349	E105	143
R346	E29	32

FIGURE 3 LG3-RBD hydrogen-bond pairs and percentage of occupancies. (a) Inter-protein hydrogen bonds made at the LG3-RBD interface calculated from the last 200 ns of the 600 ns trajectory. The amino acid residues involved in H-bonds and their %occupancies are shown in (b) and (c). If multiple significant H-bonds are formed between the same amino acid pairs, the total %occupancy can exceed 100%.

depend on a number of other factors. Interface analysis with PIsToN shows that LG3-RBD interface when not complexed with ACE2 is favorable compared to when complexed with ACE2 (Table S2), though longer simulations (especially for the ACE2-bound complex) may reveal similar binding scores.

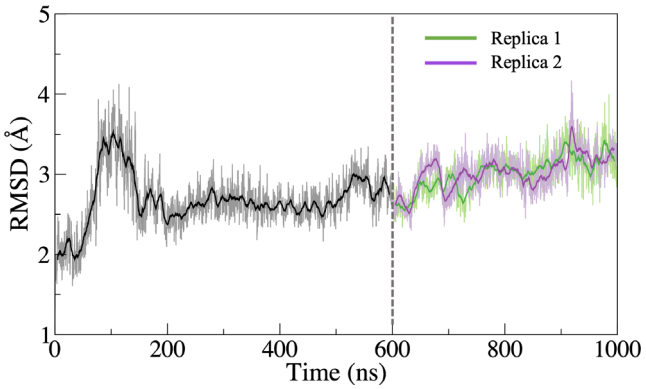

FIGURE 4 Root mean square deviation (RMSD) of the LG3-RBD complex. The dotted line at 600 ns represents the beginning of the extended simulations of replica 1 and replica 2, run for 400 ns each.

3.4 | Perlecan LG3 binds to SARS-CoV-2 RBD

Surface plasmon resonance experiments were conducted to experimentally validate the direct binding of SARS-CoV-2 RBD-Wt to LG3 and quantify the direct binding of LG3 with SARS-CoV-2 RBD. As mentioned previously, we utilized a CM5 chip to immobilize LG3 using standard amine coupling chemistry. hACE2 was immobilized on the CM5 chip surface using the same surface chemistry as used for LG3. hACE2 served as a positive control ligand in SPR experiments. Figure 6 below shows direct bindings of SARS-CoV-2 RBD-Wt to both immobilized LG3 and hACE2.

As shown in Figure 6a, SARS-CoV-2 RBD-Wt binds to LG3 in a concentration-dependent manner. A K_D value of ~72 nM was obtained when experimental SPR sensorgrams (blue continuous lines) were fitted (dashed red lines) to a 1:1 kinetics binding model. As expected, SARS-CoV-2 RBD-Wt is also bound to hACE2 Figure 6b with a K_D value of ~19 nM. We also repeated the experiment for SARS-CoV-2 RBD-Wt binding to immobilized LG3 and obtained a K_D value of ~76 nM. The data are shown in the supplementary information (Text S1, Figures S2 and S3).

(a)

RBD ↓ \ ← ACE2 →	D30	E35	Y41	Q42	Y83	K353
K417	73					
N487					76	
Q493		49				
Q498				59		
T500			59			
G502						87

(b)

RBD w LG3 ↓ \ ← ACE2 →	Q24	D30	K31	H34	E37	Y41	Y83	K353
K417		86						
Y453				33				
A475	53							
S477	78							
N487							76	
Q493			24					
T500						59		
G502								78
Y505					88			

(c)

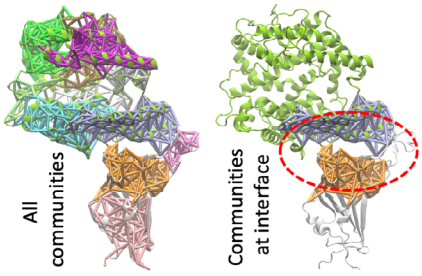

(d)

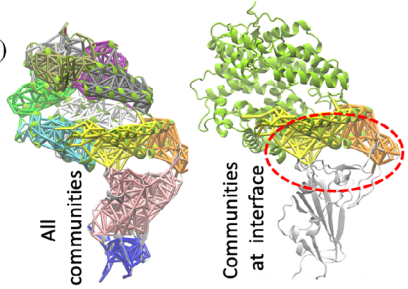

(e)

Connections at the RBD-ACE2 interface in the RBD-ACE2 system	
RBD	ACE2
N501	K353
G502	K353, G354
Y505	K353, G354
Y489	T27, F28, K31, Y83
F486	L79, M82, Y83
A475	Q24, T27
F456	T27, D30, K31
Total Connections = 17	

(f)

Connections at the RBD-ACE2 interface in the LG3-RBD-ACE2 system	
RBD	ACE2
T500	Y41, N330, D355, R357
G502	K353, G354
Y505	E37, K353, G354, R393
Y489	K31, F28, T27
N487	Q24, Y83
F486	L79, M82, Y83
S477	Q24
G476	S19, Q24
A475	T27, Q24
Y473	T27
Total Connections = 24	

FIGURE 5 LG3-RBD-ACE2 complex modeling. RBD-ACE2 interfacial hydrogen bonding pairs and their % occupancies (for H-bond occupancy >20% only) (a) in the absence of LG3 (b) and in the presence of LG3 bound to the RBD. Dynamic network analysis showing the connections between the C_α atoms of the RBD and ACE2 (c) in the absence of LG3 and (d) in the presence of LG3. Important C_α connections at the RBD-ACE2 interface in the (e) LG3-RBD and (f) LG3-RBD-ACE2 systems, respectively.

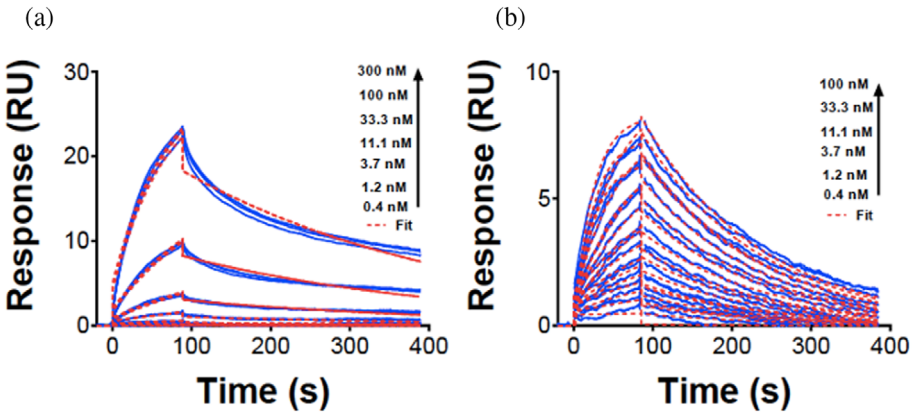

FIGURE 6 Perlecan LG3 binds to SARS-CoV-2 RBD. Binding of SARS-CoV-2 RBD-Wt with both (a) LG3 and (b) hACE2. SPR sensorgrams showing concentration-dependent binding of SARS-CoV-2 RBD-Wt to immobilize (a) LG3 and (b) hACE2. Blue continuous lines are experimental data and dotted red lines are fits to the 1:1 kinetics binding model.

4 | DISCUSSION

Understanding the mechanisms by which SARS-CoV-2 obtains entry into host cells and the factors involved in viral infectivity is paramount to understanding viral pathogenesis and our ability to generate effective therapeutic interventions. While it is known that SARS-CoV-2 enters host cells via binding ACE2 (Hoffmann et al., 2020; Lan et al., 2020; Letko et al., 2020; Tian et al., 2020; Walls et al., 2020), other cell surfaces and nearby biomolecules such as ECM proteins have also shown a binding affinity for the SARS-CoV-2 spike protein RBD, although the extent to which these molecules modulate infectivity is still unclear (De Pasquale et al., 2021; Huang et al., 2022; Jayaprakash & Surolia, 2021; Lo et al., 2022; Mehdipour & Hummer, 2021; Nguyen et al., 2021; Yu et al., 2020). As recent studies have suggested that negatively charged heparan sulfate proteoglycans may act as a cofactor for SARS-CoV-2 binding to ACE2 known to have significant effects on vascular function and vascular barriers (Biering et al., 2022; Hashimoto et al., 2022; Martínez-Salazar et al., 2022), we sought to characterize this interaction with the c-terminal LG3 subdomain of perlecan domain V. To date, no conclusive studies have been conducted investigating the potential role that perlecan LG3 may have in SARS-CoV-2 pathogenesis.

In this work, we investigated the binding interactions between SARS-CoV-2 spike protein RBD and perlecan LG3 to determine its potential role in viral cellular attachment and potential entry into host cells. We used molecular modeling simulations and SPR to elucidate potential interactions between SARS-CoV-2 RBD with ACE2 and LG3, performing molecular docking to select the best candidate complexes and combined their results with MD simulations to investigate LG3 interactions with the spike protein RBD with and without the presence of ACE2. We found that SARS-CoV-2 RBD binds to LG3 and confirmed these interactions experimentally via SPR. Several new hydrogen-bond pairs were observed in the presence of LG3. Interestingly, Y505-E37 is a prominent hydrogen bond between RBD and ACE2 in the LG3-RBD-ACE2 complex but it is not observed in the RBD-ACE2 complex without LG3. These observations suggest that RBD binding with perlecan LG3 may facilitate the spike protein attachment to the host cell not only by increasing the chances for RBD to find ACE2, but also by enhancing the RBD-ACE2 interactions.

Other factors may contribute to SARS-CoV-2 RBD binding to ACE2 in the presence of LG3, which this study did not address. For example, it is known that RBD-ACE2 interactions can be affected by mutations on the spike protein as found in subsequent viral strains of SARS-CoV-2 (Baral et al., 2021; da Costa et al., 2022; Hossen et al., 2022; Starr et al., 2020; Tian et al., 2021; Wu et al., 2022), in the presence of inhibitors (Bertoglio et al., 2021; Chen et al., 2021; Jiang et al., 2020; Jiang et al., 2021; Yang et al., 2020; Yin et al., 2022), and through structural variations in ACE2 (Hussain et al., 2020). Future work therefore should explore these factors to determine the extent of perlecan LG3 to alter viral binding outcomes relevant to SARS-CoV-2 pathophysiology.

Finally, as LG3 exists as either a part of perlecan found primarily within vascular basement membranes or as a proteolytically cleaved protein in circulation (Parker et al., 2012) which exerts considerable effect on blood vessel growth through both pro- and anti-angiogenic mechanisms (Biose et al., 2022; Clarke et al., 2012; Lee et al., 2011; Segev et al., 2004), our results suggest that LG3 may play a role in SARS-CoV-2 vascular barrier disruption as observed by others (Biering et al., 2022). This may explain, in part, the predominant vasculopathy of COVID-19 pathogenesis (Flaumenhaft et al., 2022), which we hypothesize that perlecan LG3 may play and previously unrecognized but significant role. Future experiments elucidating the role perlecan LG3 has

in vivo to SARS-CoV-2 pathogenesis would provide new insights into both the mechanism of SARS-CoV-2 infection and may provide additional potential targets for the development of new therapeutics to prevent or treat viral infectivity and subsequent clinical sequelae. We finally highlight the importance of understanding the complex interactions between viruses and host cells and the role of ECM proteins in viral pathogenesis. Further studies are needed to experimentally validate the computationally identified putative binding residues as well as to explore the clinical implications of these findings and to develop new approaches for preventing and treating COVID-19.

5 | CONCLUSION

While the ACE2 receptor has been recognized as the primary entry point for the virus, the involvement of various cell surface ECM proteins in the binding process has remained unexplored. This study provides strong data to suggest that the ECM protein perlecan LG3 may play an important role in SARS-CoV-2 viral attachment, combining molecular modeling simulations and SPR experiments to probe the significance of the binding interactions between SARS-CoV-2 RBD and LG3. Our results demonstrate the existence of these interactions and provide crucial insights into the stability and dynamics of the complexes formed. Importantly, this research hints at the possible impact that perlecan LG3 has on viral cellular attachment, host cell entry, and vascular barrier disruption, given that LG3 is found in the vascular basement membrane and can circulate as a proteolytically cleaved protein. In a broader context, this study underscores the complexity of viral interactions with host cells and highlights the pivotal role played by ECM proteins in viral pathogenesis. These findings contribute to our growing knowledge of SARS-CoV-2 infection mechanisms and may provide critical insight into SARS-CoV-2 pathophysiology which may eventually enhance the development of innovative therapeutics to mitigate viral infectivity and its clinical consequences.

AUTHOR CONTRIBUTIONS

Conceptualization: Timothy E. Gressett, Gregory Bix, Md Lokman Hossen, Purushottam B. Tiwari, and Prem Chapagain; methodology: Md Lokman Hossen, Prem Chapagain, Timothy E. Gressett, Purushottam B. Tiwari, and Gregory Bix; validation and formal analysis: Md Lokman Hossen, Prem Chapagain, and Purushottam B. Tiwari, Hugo Perez; data curation: Md Lokman Hossen and Timothy E. Gressett; writing–original draft preparation: Md Lokman Hossen and Timothy E. Gressett; writing–review and editing: Timothy E. Gressett, Gregory Bix, Md Lokman Hossen, Prem Chapagain, Grant Talkington, Milla Volic, and Purushottam B. Tiwari; supervision and project administration: Gregory Bix and Prem Chapagain; funding acquisition: Gregory Bix, Prem Chapagain. All authors have read and agreed to the published version of the manuscript.

ACKNOWLEDGMENTS

The experimental SPR sensorgrams were measured using a Biacore T200 instrument and were evaluated using the Biacore T200 evaluation software version 1.0 available in the Biacore Molecular Interaction Shared Resource (BMISR) facility at Georgetown University. The BMISR is supported by NIH grant P30CA51008.

CONFLICT OF INTEREST STATEMENT

The authors declare no conflicts of interest.

ORCID

Prem Chapagain https://orcid.org/0000-0002-0999-4975

REFERENCES

Baral P, Bhattarai N, Hossen ML, Stebliankin V, Gerstman BS, Narasimhan G, et al. Mutation-induced changes in the receptor-binding interface of the SARS-CoV-2 delta variant B. 1.617. 2 and implications for immune evasion. Biochem Biophys Res Commun. 2021;574:14–9.

Berman HM, Westbrook J, Feng Z, Gilliland G, Bhat TN, Weissig H, et al. The protein data bank. Nucleic Acids Res. 2000;28(1):235–42.

Bertoglio F, Meier D, Langreder N, Steinke S, Rand U, Simonelli L, et al. SARS-CoV-2 neutralizing human recombinant antibodies selected from pre-pandemic healthy donors binding at RBD-ACE2 interface. Nat Commun. 2021;12(1):1–15.

Best RB, Zhu X, Shim J, Lopes PE, Mittal J, Feig M, et al. Optimization of the additive CHARMM all-atom protein force field targeting improved sampling of the backbone ϕ, ψ and side-chain χ1 and χ2 dihedral angles. J Chem Theory Comput. 2012;8(9):3257–73.

Biering SB, Gomes de Sousa FT, Tjang LV, Pahmeier F, Zhu C, Ruan R, et al. SARS-CoV-2 spike triggers barrier dysfunction and vascular leak via integrins and TGF-β signaling. Nat Commun. 2022;13(1):7630.

Biose IJ, Rutkai I, Clossen B, Gage G, Schechtman K, Adkisson HDT, et al. Recombinant human perlecan DV and its LG3 subdomain are neuroprotective and acutely functionally restorative in severe experimental ischemic stroke. Transl Stroke Res. 2023;14(6):941–54.

Brodowski M, Pierpaoli M, Janik M, Kowalski M, Ficek M, Slepski P, et al. Enhanced susceptibility of SARS-CoV-2 spike RBD protein assay targeted by cellular receptors ACE2 and CD147: multivariate data analysis of multisine impedimetric response. Sens Actuators B Chem. 2022;370:132427.

Chen RH, Yang LJ, Hamdoun S, Chung SK, Lam CW-K, Zhang KX, et al. 1, 2, 3, 4, 6-pentagalloyl glucose, a RBD-ACE2 binding inhibitor to prevent SARS-CoV-2 infection. Front Pharmacol. 2021;12:634176.

Clarke DN, Al Ahmad A, Lee B, Parham C, Auckland L, Fertala A, et al. Perlecan domain V induces VEGf secretion in brain endothelial cells through integrin alpha5beta1 and ERK-dependent signaling pathways. PloS One. 2012;7(9):e45257.

Clausen TM, Sandoval DR, Spliid CB, Pihl J, Perrett HR, Painter CD, et al. SARS-CoV-2 infection depends on cellular Heparan sulfate and ACE2. Cell. 2020;183(4):1043–57.e15.

da Costa CHS, de Freitas CAB, Alves CN, Lameira J. Assessment of mutations on RBD in the spike protein of SARS-CoV-2 alpha, delta and omicron variants. Scientif Rep. 2022;12(1):1–10.

Darden T, York D, Pedersen L. Particle mesh Ewald: an N· log (N) method for Ewald sums in large systems. J Chem Phys. 1993;98(12):10089–92.

De Pasquale V, Quiccione MS, Tafuri S, Avallone L, Pavone LM. Heparan sulfate proteoglycans in viral infection and treatment: a special focus on SARS-CoV-2. Int J Mol Sci. 2021;22(12):6574.

Essmann U, Perera L, Berkowitz ML, Darden T, Lee H, Pedersen LG. A smooth particle mesh Ewald method. J Chem Phys. 1995;103(19):8577–93.

Feller SE, Zhang Y, Pastor RW, Brooks BR. Constant pressure molecular dynamics simulation: the Langevin piston method. J Chem Phys. 1995;103(11):4613–21.

Flaumenhaft R, Enjyoji K, Schmaier AA. Vasculopathy in COVID-19. Blood. 2022;140(3):222–35.

Gonzalez EM, Reed CC, Bix G, Fu J, Zhang Y, Gopalakrishnan B, et al. BMP-1/tolloid-like metalloproteases process endorepellin, the angiostatic C-terminal fragment of perlecan. J Biol Chem. 2005;280(8):7080–7.

Gubbiotti MA, Neill T, Iozzo RV. A current view of perlecan in physiology and pathology: a mosaic of functions. Matrix Biol. 2017;57-58:285–98.

Hashimoto R, Takahashi J, Shirakura K, Funatsu R, Kosugi K, Deguchi S, et al. SARS-CoV-2 disrupts respiratory vascular barriers by suppressing Claudin-5 expression. Sci Adv. 2022;8(38):e6783.

Hayes AJ, Farrugia BL, Biose IJ, Bix GJ, Melrose J. Perlecan, a multi-functional, cell-instructive, matrix-stabilizing proteoglycan with roles in tissue development has relevance to connective tissue repair and regeneration. Front Cell Dev Biol. 2022;10:856261.

Hoffmann M, Kleine-Weber H, Schroeder S, Krüger N, Herrler T, Erichsen S, et al. SARS-CoV-2 cell entry depends on ACE2 and TMPRSS2 and is blocked by a clinically proven protease inhibitor. Cell. 2020;181:271–80.e8.

Hossen ML, Baral P, Sharma T, Gerstman B, Chapagain P. Significance of the RBD mutations in the SARS-CoV-2 omicron: from spike opening to antibody escape and cell attachment. Phys Chem Chem Phys. 2022;24(16):9123–9.

Huang Y, Harris BS, Minami SA, Jung S, Shah PS, Nandi S, et al. SARS-CoV-2 spike binding to ACE2 is stronger and longer ranged due to glycan interaction. Biophys J. 2022;121(1):79–90.

Humphrey W, Dalke A, Schulten K. VMD: visual molecular dynamics. J Mol Graph. 1996;14(1):33–8.

Hussain M, Jabeen N, Raza F, Shabbir S, Baig AA, Amanullah A, et al. Structural variations in human ACE2 may influence its binding with SARS-CoV-2 spike protein. J Med Virol. 2020;92(9):1580–6.

Iacobucci I, Monaco V, Cane L, Bibbo F, Cioffi V, Cozzolino F, et al. Spike S1 domain interactome in non-pulmonary systems: a role beyond the receptor recognition. Front Mol Biosci. 2022;9:975570.

Jayaprakash NG, Surolia A. Spike protein and the various cell-surface carbohydrates: an interaction study. ACS Chem Biol. 2021;17(1):103–17.

Jiang S, Hillyer C, Du L. Neutralizing antibodies against SARS-CoV-2 and other human coronaviruses. Trends Immunol. 2020;41(5):355–9.

Jiang S, Zhang X, Du L. Therapeutic antibodies and fusion inhibitors targeting the spike protein of SARS-CoV-2. Expert Opin Ther Targets. 2021;25(6):415–21.

Jo S, Kim T, Iyer VG, Im W. CHARMM-GUI: a web-based graphical user interface for CHARMM. J Comput Chem. 2008;29(11):1859–65.

Jorgensen WL, Chandrasekhar J, Madura JD, Impey RW, Klein ML. Comparison of simple potential functions for simulating liquid water. J Chem Phys. 1983;79(2):926–35.

Kadam SB, Sukhramani GS, Bishnoi P, Pable AA, Barvkar VT. SARS-CoV-2, the pandemic coronavirus: molecular and structural insights. J Basic Microbiol. 2021;61(3):180–202.

Lan J, Ge J, Yu J, Shan S, Zhou H, Fan S, et al. Structure of the SARS-CoV-2 spike receptor-binding domain bound to the ACE2 receptor. Nature. 2020;581(7807):215–20.

Le BV, Kim H, Choi J, Kim J-H, Hahn M-J, Lee C, et al. Crystal structure of the LG3 domain of endorepellin, an angiogenesis inhibitor. J Mol Biol. 2011;414(2):231–42.

Lee B, Clarke D, Al Ahmad A, Kahle M, Parham C, Auckland L, et al. Perlecan domain V is neuroprotective and proangiogenic following ischemic stroke in rodents. J Clin Invest. 2011;121(8):3005–23.

Lee J, Cheng X, Swails JM, Yeom MS, Eastman PK, Lemkul JA, et al. CHARMM-GUI input generator for NAMD, GROMACS, AMBER, OpenMM, and CHARMM/OpenMM simulations using the CHARMM36 additive force field. J Chem Theory Comput. 2016;12(1):405–13.

Letko M, Marzi A, Munster V. Functional assessment of cell entry and receptor usage for SARS-CoV-2 and other lineage B betacoronaviruses. Nat Microbiol. 2020;5(4):562–9.

Lo MW, Amarilla AA, Lee JD, Albornoz EA, Modhiran N, Clark RJ, et al. SARS-CoV-2 triggers complement activation through interactions with heparan sulfate. Clin Transl Immunol. 2022;11(8):e1413.

Martinez JR, Dhawan A, Farach-Carson MC. Modular proteoglycan perlecan/*HSPG2*: mutations, phenotypes, and functions. Genes (Basel). 2018;9(11):556.

Martínez-Salazar B, Holwerda M, Stüdle C, Piragyte I, Mercader N, Engelhardt B, et al. COVID-19 and the vasculature: current aspects and long-term consequences. Front Cell Dev Biol. 2022;10:824851.

Martyna GJ, Tobias DJ, Klein ML. Constant pressure molecular dynamics algorithms. J Chem Phys. 1994;101(5):4177–89.

Mehdipour AR, Hummer G. Dual nature of human ACE2 glycosylation in binding to SARS-CoV-2 spike. Proc Natl Acad Sci. 2021;118(19):e2100425118.

Melo MC, Bernardi RC, de la Fuente-Nunez C, Luthey-Schulten Z. Generalized correlation-based dynamical network analysis: a

new high-performance approach for identifying allosteric communications in molecular dynamics trajectories. J Chem Phys. 2020;153(13):134104.

Melrose J. Perlecan, a modular instructive proteoglycan with diverse functional properties. Int J Biochem Cell Biol. 2020;128:105849.

Nguyen K, Chakraborty S, Mansbach RA, Korber B, Gnanakaran S. Exploring the role of glycans in the interaction of SARS-CoV-2 RBD and human receptor ACE2. Viruses. 2021;13(5):927.

Norris EG, Pan XS, Hocking DC. Receptor binding domain of SARS-CoV-2 is a functional alphav-integrin agonist. J Biol Chem. 2023;299(3):102922.

Parker TJ, Sampson DL, Broszczak D, Chng YL, Carter SL, Leavesley DI, et al. A fragment of the LG3 peptide of endorepellin is present in the urine of physically active mining workers: a potential marker of physical activity. PloS One. 2012;7(3):e33714.

Phillips J, Braun R, Wang W, Gumbart J, Tajkhorshid E, Villa E, et al. Scalable molecular dynamics with NAMD. J Comput Chem. 2005;26(16):1781–802.

Roberts E, Eargle J, Wright D, Luthey-Schulten Z. MultiSeq: unifying sequence and structure data for evolutionary analysis. BMC Bioinfo. 2006;7(1):1–11.

Ryckaert J-P, Ciccotti G, Berendsen HJ. Numerical integration of the Cartesian equations of motion of a system with constraints: molecular dynamics of n-alkanes. J Comput Phys. 1977;23(3):327–41.

Segev A, Nili N, Strauss BH. The role of perlecan in arterial injury and angiogenesis. Cardiovasc Res. 2004;63(4):603–10.

Shang J, Ye G, Shi K, Wan Y, Luo C, Aihara H, et al. Structural basis of receptor recognition by SARS-CoV-2. Nature. 2020;581(7807):221–4.

Starr TN, Greaney AJ, Hilton SK, Ellis D, Crawford KH, Dingens AS, et al. Deep mutational scanning of SARS-CoV-2 receptor binding domain reveals constraints on folding and ACE2 binding. Cell. 2020;182(5):1295–310. e20.

Stebliankin V, Shirali A, Baral P, Shi J, Chapagain P, Mathee K, et al. Evaluating protein binding interfaces with transformer networks. Nat Mach Intell. 2023;5(9):1042–53.

Tian F, Tong B, Sun L, Shi S, Zheng B, Wang Z, et al. N501Y mutation of spike protein in SARS-CoV-2 strengthens its binding to receptor ACE2. Elife. 2021;10:e69091.

Tian X, Li C, Huang A, Xia S, Lu S, Shi Z, et al. Potent binding of 2019 novel coronavirus spike protein by a SARS coronavirus-specific human monoclonal antibody. Emerg Microb Infect. 2020;9(1):382–5.

Vanommeslaeghe K, Hatcher E, Acharya C, Kundu S, Zhong S, Shim J, et al. CHARMM general force field: a force field for drug-like molecules compatible with the CHARMM all-atom additive biological force fields. J Comput Chem. 2010;31(4):671–90.

Walls AC, Park Y-J, Tortorici MA, Wall A, McGuire AT, Veesler D. Structure, function, and antigenicity of the SARS-CoV-2 spike glycoprotein. Cell. 2020;181(2):281–92. e6.

Wrapp D, Wang N, Corbett KS, Goldsmith JA, Hsieh C-L, Abiona O, et al. Cryo-EM structure of the 2019-nCoV spike in the prefusion conformation. Science. 2020;367(6483):1260–3.

Wu L, Zhou L, Mo M, Liu T, Wu C, Gong C, et al. SARS-CoV-2 omicron RBD shows weaker binding affinity than the currently dominant delta variant to human ACE2. Signal Transduct Target Ther. 2022;7(1):1–3.

Yan Y, Tao H, He J, Huang S-Y. The HDOCK server for integrated protein–protein docking. Nat Protoc. 2020;15(5):1829–52.

Yang J, Petitjean SJ, Koehler M, Zhang Q, Dumitru AC, Chen W, et al. Molecular interaction and inhibition of SARS-CoV-2 binding to the ACE2 receptor. Nat Commun. 2020;11(1):1–10.

Yin W, Xu Y, Xu P, Cao X, Wu C, Gu C, et al. Structures of the omicron spike trimer with ACE2 and an anti-omicron antibody. Science. 2022;375(6584):1048–53.

Yu J, Yuan X, Chen H, Chaturvedi S, Braunstein EM, Brodsky RA. Direct activation of the alternative complement pathway by SARS-CoV-2 spike proteins is blocked by factor D inhibition. Blood. 2020;136(18):2080–9.

Zhang JJ, Dong X, Liu GH, Gao YD. Risk and protective factors for COVID-19 morbidity, severity, and mortality. Clin Rev Allergy Immunol. 2023;64(1):90–107.

SUPPORTING INFORMATION

Additional supporting information can be found online in the Supporting Information section at the end of this article.

How to cite this article: Gressett TE, Hossen ML, Talkington G, Volic M, Perez H, Tiwari PB, et al. Molecular interactions between perlecan LG3 and the SARS-CoV-2 spike protein receptor binding domain. Protein Science. 2024;33(1):e4843. https://doi.org/10.1002/pro.4843